Population of ^{10}Li by fragmentation

M. Thoennessen, S. Yokoyama,* A. Azhari,† T. Baumann,‡ J. A. Brown,§ A. Galonsky, P. G. Hansen, J. H. Kelley,‖ R. A. Kryger, E. Ramakrishnan,† and P. Thirolf¶

National Superconducting Cyclotron Laboratory and Department of Physics & Astronomy, Michigan State University, East Lansing, Michigan 48824

(Received 2 September 1998)

The decay structure of the particle-unstable nucleus ^{10}Li was studied using the method of sequential neutron decay spectroscopy (SNDS) at 0°. The decay energies of ^{10}Li can be derived from the relative velocity spectrum of the ^{9}Li daughter and the neutron measured in coincidence. Evidence for low-lying *s*-wave strength was observed with a scattering length of <-20 fm, corresponding to a peak energy of <50 keV. [S0556-2813(99)06201-9]

PACS number(s): 27.20.+n, 25.70.Mn, 21.10.Dr

I. INTRODUCTION

The detailed structure of the neutron unbound nucleus ^{10}Li continues to be of high experimental [1–6] as well as theoretical interest [7–9]. The spin and parity of the ^{10}Li ground state is essential for the understanding of the two-neutron halo nucleus ^{11}Li. The simple shell model predicts the ground state to be a $p_{1/2}$ neutron coupled with a $p_{3/2}$ proton to either a 1^+ or a 2^+ state. However, ^{10}Li is a member of the $N=7$ isotones where with decreasing mass the $s_{1/2}$ state becomes lower in energy relative to the $p_{1/2}$ state and forms the ground state in ^{11}Be. If this trend continues towards the lighter nuclei, ^{10}Li should have a ground state where the $p_{3/2}$ proton is coupled to the $s_{1/2}$ neutron to form a 1^- or a 2^- state [10,11].

Although most theoretical calculations predict the shell inversion [11], it is still controversial [7,12]. Experimentally, several measurements report the observation of *p*-wave resonances. From the first measurement of Wilcox *et al.* which reported a state at 800 ± 250 keV [13], to the more recent data of Bohlen (420 ± 50 keV and 800 ± 80 keV) [14], Young (538 ± 62 keV) [15], and Bohlen (240 ± 60 keV and 530 ± 60 keV) [4] the situation is not clear. In Ref. [4] the authors report that the reanalysis of the data of their earlier paper [14] showed only one peak at 530 keV consistent with Young's result. The preliminary analysis of an experiment by Caggiano *et al.* [6] confirms the observation of the state reported by Young *et al.* [15]. Thus, it seems that there could be potentially two *p*-states at ~240 keV and ~540 keV which could correspond to the 1^+ and 2^+ state.

The observation of the *s*-wave is even more complicated. A neutron *s*-wave state in the continuum is not contained by any barrier and thus is not a real resonance but its low-energy properties can most conveniently be described in terms of a scattering length. However, it is sometimes referred to as a virtual resonance. The first observation and interpretation of low-lying strength in terms of a virtual *s*-wave resonance was shown by Kryger *et al.* [16]. A previous pion absorption measurement observed a peak at 150 keV [17], however, it is most likely associated with the *p* strength discussed above. Kryger *et al.* populated light neutron rich nuclei by fragmentation of ^{18}O, and deduced the relative decay energy from a coincidence measurement of ^{9}Li and a neutron. Since this first experiment, several other experiments showed independent evidence for low lying strength in ^{10}Li [2,3,5,15,18–20].

We repeated the experiment of Kryger *et al.* with improved energy resolution in order to establish more stringent limits for the *s*-wave parameters. We analyzed the data in terms of the scattering length of the system neutron plus ^{9}Li arising from the breakup of ^{18}O. We also aimed to determine if the central peak observed by Kryger *et al.* could potentially be interpreted as the recently observed 240 keV *p*-wave [4].

II. EXPERIMENTAL SETUP

The experiment was performed at the National Superconducting Cyclotron Laboratory (NSCL). An ^{18}O beam with a kinetic energy of 80 MeV/nucleon provided by the K1200 cyclotron bombarded a 94 mg/cm^2 thick ^{9}Be target located in front of a quadrupole-dipole magnet combination (Fig. 1). The magnets were tuned to optimize the detection rate of $A/Z=3$ fragments (^{3}H,^{6}He,^{9}Li,^{12}Be, and ^{15}B) in a fragment telescope located at 11° from the primary beam axis. The telescope consisted of a thin fast plastic timing detector (25.4 μm thick), a 2.54 cm thick copper collimator, three quadrant segmented silicon ΔE detectors (1016 μm, 486 μm, and 478 μm thick, 5.0 cm$\times$5.0 cm), and an array of nine CsI(Tl) E detectors. The flight path of the fragments was 6.0 m. The nonreacting primary beam was bent into the

*Present address: Department of Physics, University of Michigan, Ann Arbor, MI 48109.

†Present address: Cyclotron Institute, Texas A&M University, College Station, TX 77843.

‡Present address: Gesellschaft für Schwerionenforschung, D-64291 Darmstadt, Germany.

§Present address: Department of Physics & Astronomy, Millikin University, Decatur, IL 62522.

‖Present address: Triangle University Nuclear Laboratory, Duke University, Durham, NC 27708.

¶Present address: Sektion Physik der Universität München, D-85748 Garching, Germany.

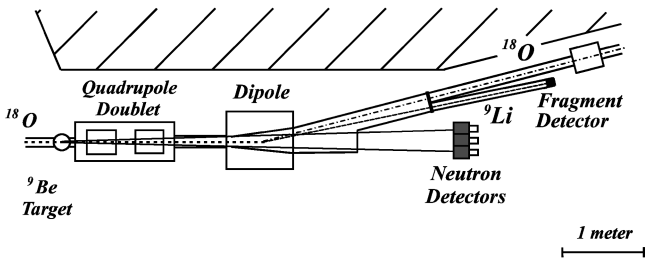

FIG. 1. Experimental setup.

14° beamline and was collected in a shielded Faraday cup located in a separate room 25 m downstream from the target to reduce the background. The neutrons from the fragmentation and from the neutron decay of the fragmentation products were detected in an array of five NE213 liquid scintillator detectors at 0 °. The flight path of the neutrons was 5.8 m.

The fragments of ^{6}He and ^{9}Li were identified in two-dimensional plots of ΔE-E and ΔE–time of flight (TOF). Neutrons and γ rays in the neutron detector were identified and separated by pulse shape discrimination [21]. The fragment velocity was calculated directly from the fragment energy while the neutron velocity was obtained from the TOF of the neutrons relative to the fragments and then corrected for the fragment TOF.

III. DATA ANALYSIS

A. *p*- and *s*-wave simulations

This technique where the neutrons and the fragments are detected in a collinear geometry with a small angular acceptance is referred to as sequential neutron decay spectroscopy (SNDS) [22]. From the extracted neutron and fragment TOFs, the relative velocity spectrum can be calculated which is directly related to the decay energy of the initial state; $E_{\mathrm{decay}}=\frac{1}{2}\mu v_{\mathrm{rel}}^{2}$ where μ is the reduced mass.

The measured relative velocity spectra were compared with Monte Carlo simulations of the calculated relative velocity spectra. The decay direction was assumed to be isotropic in the center of mass (c.m.) reference frame.

The *p*-wave resonances were simulated assuming a Breit-Wigner line shape of the form [23]

$$\frac{d\sigma}{dE}\propto\frac{\Gamma(E)^{2}}{(E-E_{r})^{2}+\frac{1}{4}\Gamma(E)^{2}}, \tag{1}$$

where $\Gamma(E)=[k\mathrm{P}_{l}(E)/k_{r}\mathrm{P}_{l}(E_{r})]\Gamma_{r}$, $\mathrm{P}_{l}(E)$ is the l-dependent neutron penetrability function, and the index r indicate values at the resonance energy.

The *s*-wave states were analyzed in a potential-model approach similar to that of [20]. The calculation is based on the sudden approximation. It assumes that a scattering state of a neutron and ^{9}Li is created at the instant of the breakup reaction, so that the outcome is obtained by expanding its wave function into continuum eigenstates that are numerical solutions to the Schrödinger equation. The interaction in the final state is approximated by a Woods-Saxon potential with parameters $r_{0}=1.15$ fm and $a=0.5$ fm. For *s* states, the well depth is chosen to reproduce selected values of the *s*-wave scattering length a_{s}, and for *p* states to place the resonance at the desired energy. The probability of a given momentum of the final state is now given by the square of the overlap with the initial state. The advantage of parametrization of the continuum states in this way is that the results for neutrons of low energy are essentially independent of the details of the potential, so that the ^{10}Li states are characterized by a single real parameter. We have verified this feature by comparing the results with analytical calculations for a square well. This simplification is possible because the states involved are predominantly of single-particle nature.

The essential problem is to specify a wave function for the initial state. We take as the starting point the Goldhaber model [24], which assumes that the momentum of a given fragment in the projectile rest system is that pre-existing in the projectile. For the fragmentation of a projectile with mass number A, the spreading width σ of the momentum of a fragment with mass A_{F} is given by the expression

$$\sigma=\sigma_{0}\sqrt{\frac{A_{F}(A-A_{F})}{A-1}},$$

where the parameter σ_{0} is 70–90 MeV/c at high beam energies. This shows that the average velocity of the neutron is approximately four times that of ^{9}Li, so that it is a good approximation to consider ^{9}Li at rest in the projectile frame. This means that the angular momentum of the resulting continuum state must be identical to that of the initial state. (This makes the calculation simpler than that of [20], where the low binding of the ^{11}Be neutron made the two velocities comparable. It therefore became necessary to carry out an expansion in angular-momentum eigenstates in the $^{9}\mathrm{Li}+n$ center-of-mass system, and subsequently to transform the result back to the projectile coordinate system.) The initial *s* and *p* states were approximated as bound states in ^{18}O and their wave functions were calculated with the Woods-Saxon potential given above. The depth of the well was adjusted to reproduce a neutron separation energy of 8 MeV. The resulting distribution is sensitive to the binding of the initial state and this dependence will be shown in Sec. III E.

The procedure used here has much in common with the use of two-particle interferometry [25,26] for extracting information about the conditions in the initial reaction complex from the final states of two particles with known interactions. Here we go the opposite way and proceed from a rather schematic model of the reaction to arrive at conclusions about the interactions between two final products. The validity of this procedure for the calculation of the *s* state of ^{10}Li is certainly debatable, however, the fact that the results for ^{7}He (see Sec. III B) agree well with the known properties of this *p*-wave resonance supports this approach.

Finally, the geometry of the detectors as well as the beamline geometry, which was calculated by raytracing through the quadrupole and dipole magnets with the code RAYTRACE [27], were taken into account for (Monte Carlo) modeling the valid events. The energy dependence of the neutron detector efficiency was calculated with the code KSUEFF [28] and folded in the calculated relative velocity spectra.

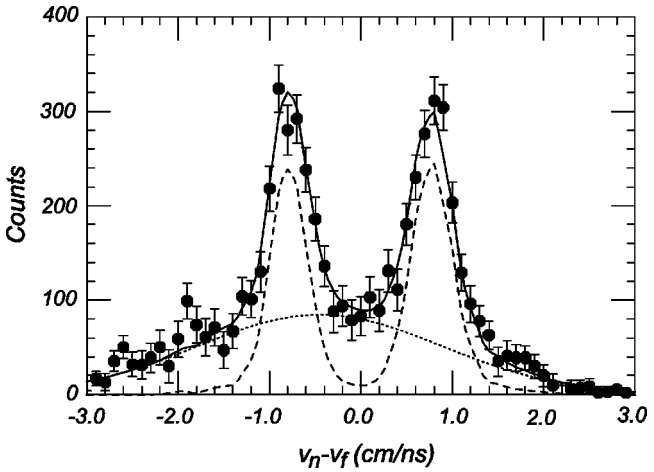

FIG. 2. Relative velocity spectrum of ^{7}He. The right and the left peak correspond to forward and backward emitted neutrons, respectively. The solid line is the result of Monte Carlo simulations with the known values of the decay of ^{7}He ($E_{\mathrm{decay}}=450$ keV,$\Gamma_{\mathrm{decay}}=160$ keV) (dashed) and an estimated background (dotted).

B. ^{7}He and calibration

The known energy and width of the ground-state decay of ^{7}He to $n+^{6}$He at $E_r=440\pm30$ keV, $\Gamma=160\pm30$ keV [29] were used to determine the resolution of the detectors. Figure 2 shows the relative velocity spectrum of $n+^{6}$He coincidence events compared to the Monte Carlo simulations. Two peaks are observed at $v_{\mathrm{rel}}\approx\pm0.8$ cm/ns on top of a broad background. Previous simulations of the background assumed a thermal neutron source of the form $\sqrt{E}\exp(-E/T)$ and resulted in a broad near-Gaussian distribution [22] when folded with the detector acceptance. The solid line in Fig. 2 shows the simulated relative velocity spectrum as a sum of the estimated Gaussian-like background (dotted) and the simulations for the decay of ^{7}He (dashed).

The resolution of the relative velocity spectrum was determined from the standard deviation of the TOF distribution for the neutron (σ_{tn}) and fragment (σ_{tf}) in the Monte Carlo simulation. The fragment velocity was calculated from the fragment energy with a TOF resolution of $\sigma_{tf}=0.057$ ns. The resolution of the neutron TOF of $\sigma_{tn}=0.70$ ns was extracted from a fit to the data. This corresponds to a substantial improvement over the experiment by Kryger *et al.* [16] where the resolutions of σ_{tf} and σ_{tn} were both 0.89 ns.

C. ^{10}Li–*s*-wave

Figure 3 shows the relative velocity spectrum of ^{10}Li. In contrast to the ^{7}He spectrum a single peak around zero relative velocity is present indicating a very low decay energy. Weak indications of two peaks at $v_{\mathrm{rel}}\approx\pm0.8$ cm/ns could correspond to the *p*-state at 540 keV. In this section the central peak is analyzed assuming an *s*-wave using the potential scattering model. In this model a neutron initially bound by 8 MeV in ^{18}O, is scattered off ^{9}Li which is produced in the fragmentation reaction. Figure 4 shows the energy distributions (top) and the resulting relative velocities (bottom) for a wide range of scattering lengths. From these simulations an upper limit of the scattering length of -20 fm was deduced. Due to the resolution of the detectors a lower limit cannot be

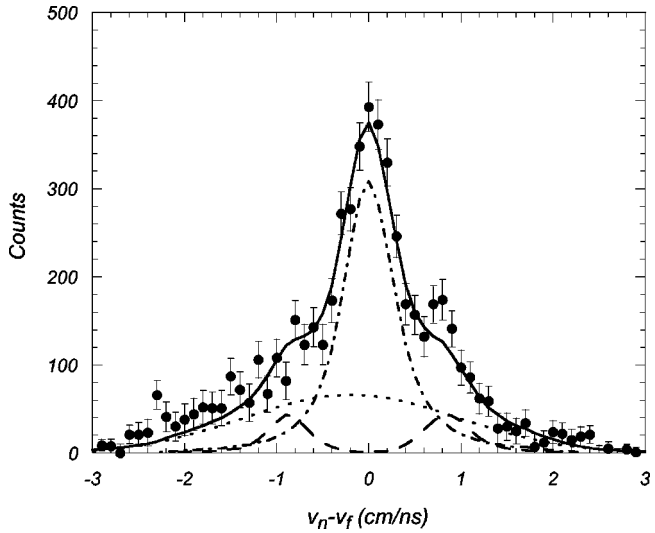

FIG. 3. Relative velocity spectrum of ^{10}Li. The Monte Carlo simulations (solid) include contributions from an *s*-wave with $a_s=-30$ fm (dot-dashed), a *p*-wave at $E_{\mathrm{decay}}=538$ keV, $\Gamma_{\mathrm{decay}}=358$ keV (dashed) and an estimated background (dotted).

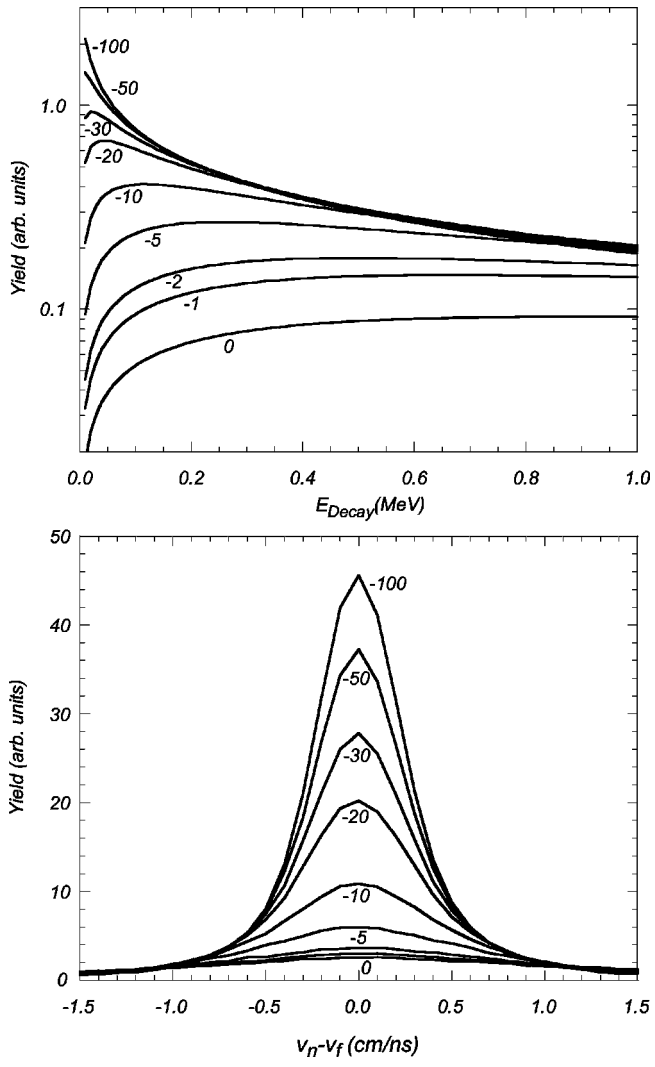

FIG. 4. Energy (top) and relative velocity (bottom) spectra for different scattering lengths.

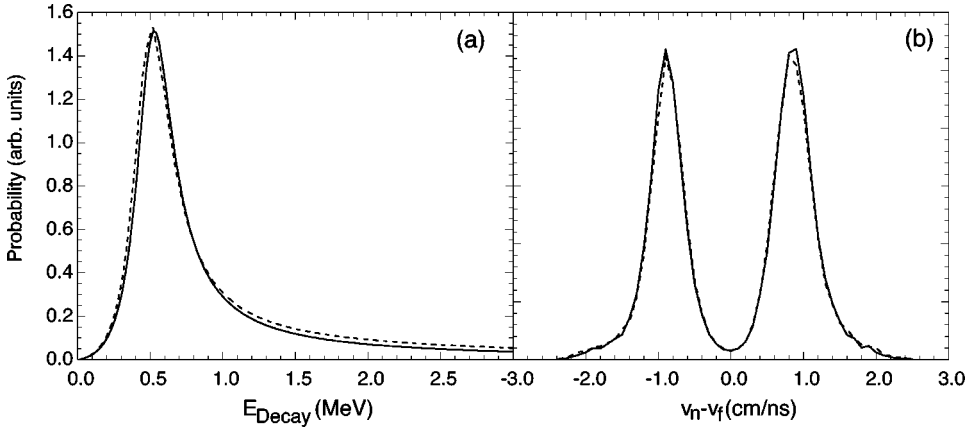

FIG. 5. Comparison of the energy (a) and the relative velocity (b) of the *p*-wave resonance calculated with the potential model (solid) and a calculation using a Breit-Wigner shape with energy and width (dashed) parameters of Ref. [34].

established and values through $-\infty$ fm are possible corresponding to very small apparent peak energies.

Figure 3 shows the results of the simulations with a scattering length of -30 fm (dot-dashed). The other contributions to the fit (solid) are the simulations for a *p*-state resonance at $E_r=538$ keV, $\Gamma=358$ keV [15] (dashed) and a Gaussian background (dotted).

The potential scattering model can also be applied to the *p*-state where it reproduced the line shapes calculated with the Breit-Wigner distribution of Eq. (1). Figure 5 shows a comparison of the energy line shape and the corresponding relative velocity spectrum of the Breit-Wigner shape (solid) and the results from the potential scattering model (dashed).

This simultaneous analysis of the *s*- and *p*-wave allows an estimate of the relative strength of the two states. In a very rough approximation it can be assumed that there are equal numbers of *p*-wave $(0p_{1/2})^2$ and *s*/*d*-wave $(1s_{1/2}/0d_{5/2})^2$ neutrons available from the break-up of ^{18}O into ^{9}Li. The ground-state of ^{18}O consists of $\sim$20% *s*-wave and $\sim$80% *d*-wave [30] and thus the relative contribution of the *s*-wave with respect to the sum of *s*- and *p*-wave strength should be $\sim$17%. Figure 6 shows the *p*-wave (47%, solid) and *s*-wave (53%, dashed) yields as a function of relative energy. These relative contributions were calculated for a scattering length of -30 fm and because of the uncertainties in the region of the *p*-state, should be taken only as an estimate. The contribution of the *s*-wave decreases with decreasing scattering lengths. For -100 fm the contributions are reversed, i.e., 47% *s*-wave and 53% *p*-wave. This seems to indicate very small scattering lengths.

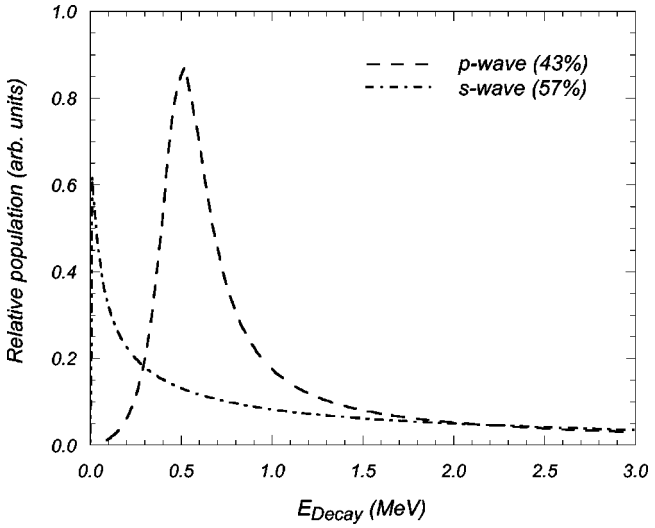

FIG. 6. Relative population of the *s*-wave (dot-dashed) and the *p*-wave (dashed) assuming the parameters from Fig. 3.

D. ^{10}Li–*p*-wave

The data clearly favor an *s*-wave for the central peak with indications of a (p)-state at $\sim$540 keV. However, the recently [4] reported *p*-state at $\sim$240 keV cannot be ruled out to be present in the data. Including this state into the simulations does not improve the quality of the fit.

Figure 7 shows the fits assuming that no *s*-wave (which corresponds to $a_s=0$ fm and is very similar to the background) is present and that the central peak is described with a *p*-state. The result of the simulations using the lower limit (180 keV) of the resonance observed in Ref. [4] with a width of $\Gamma_{res}=80$ keV is shown in (a) which clearly does not fit the data. Even increasing the width to $\Gamma_{res}=700$ keV corresponding to twice the single particle limit does not improve the fit. In Fig. 7(b) the resonance energy was reduced to 50 keV ($\Gamma_{res}=40$ keV, corresponding to the single particle limit) which represents an upper limit for a potential *p*-wave resonance to describe the central peak. This limit is substantially lower than the limit set in Ref. [16] and definitely rules out the recently observed low lying *p*-states of Ref. [4] as the origin of the central peak. It should be mentioned that the strong final-state interaction observed in Ref. [20] in the reaction ^{12}C(^{11}Be,^{9}Li+n)X, where the neutron initially is in an *s*-state, also favors an $l=0$ assignment.

The total fit of Fig. 7(b) includes the contribution from the second *p*-wave state at $E_R=538$ keV (short-dashed) [15]. If the decay spectrum of ^{10}Li contains two *p*-wave resonances, in principle interference between these states would have to be considered. The interference between overlapping continuum states is well known in neutron physics and has, for example, been observed in the β-delayed proton decay of ^{17}Ne [31]. However, in the present case the statistics at the larger decay energies is not sufficient to observe the effect of interference in the data and since the central peak is not likely to correspond to a *p*-state interference was not incorporated in the analysis.

E. Comparison with other results

The present finding of low-lying strength in terms of an *s*-wave scattering length is very similar to the recent analysis

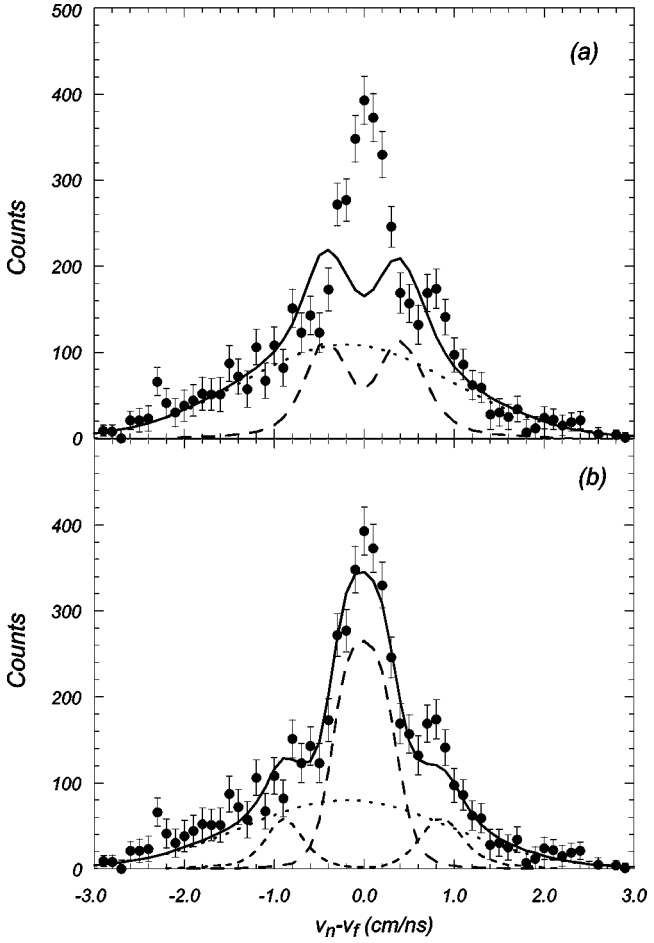

FIG. 7. Calculations assuming p-states only: (a) $E_{res}=180$ keV (lower limit of Ref. [4]), $\Gamma_{res}=80$ keV, and (b) $E_{res}=50$ keV, $\Gamma_{res}=40$ keV (long-dashed) with the additional contribution of the state of Ref. [15] at 538 keV (short-dashed).

of Bertsch *et al.* [9] for the breakup of ^{11}Li. The main difference is the initial state. In the breakup of ^{11}Li the effective one-neutron binding energy is approximately 320 keV [9], while in the breakup of ^{18}O the neutron is bound by 8 MeV. Figure 8 shows a comparison of the energy spectra for the two models for a scattering length of -5 fm. The calculations based on the parametrization of Ref. [9] (dot-dashed) are essentially identical to the present approach (dashed) for very loosely bound neutrons, here shown for a single-neutron separation energy of 280 keV. A calculation for strongly bound neutrons (dashed) shows the strong dependence of the energy distribution on the initial state. This dependence was also pointed out by Descouvemont [7]. Thus the comparison of the apparent peak energies and the scattering lengths for situations in which the state is produced in different reactions is not straightforward.

Figure 9 shows presently available data for the p- and s-states. There appear to be two p-wave resonances at $\sim$240 keV and $\sim$540 keV. However, the reaction ^{10}Be(^{12}C,^{12}N)^{10}Li [4] populated only the lower and the reactions ^{9}Be(^{13}C, ^{12}N)^{10}Li [14], ^{11}B(^{7}Li,^{8}B)^{10}Li [15] and ^{9}Be(^{9}Be,^{8}B)^{10}Li populated only the higher resonance. It is not obvious why these multiparticle transfer reactions should be so selective. There are indications of a state around

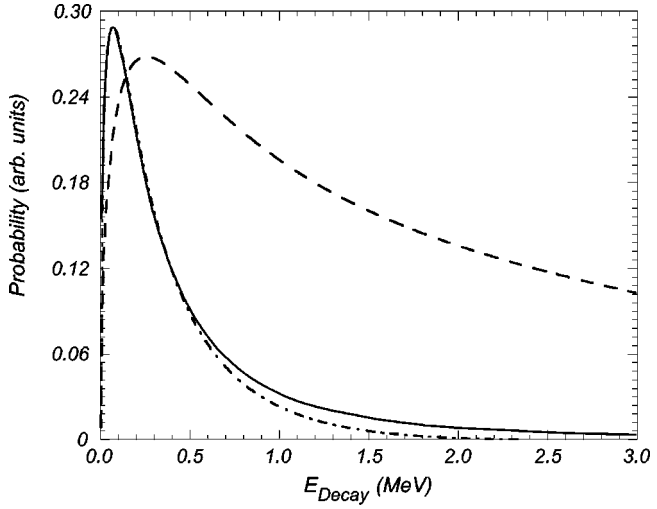

FIG. 8. Potential model calculations for a scattering length of $a_s=-5$ fm. For weakly bound neutrons (280 keV) the potential model (solid) and the parametrization of Ref. [9] (dot-dashed) are in good agreement. The energy distribution of initially more strongly bound neutrons (8 MeV) calculated with the potential model is substantially wider (dashed).

$\sim$540 keV in the present data, however another state at $\sim$240 keV cannot be ruled out.

Since the observation of the p-wave resonance around $\sim$240 keV it seems more likely that the first observation of a low-lying state by Amelin (1990) [17] which is usually mentioned as evidence for an s-wave state corresponds to this p-state.

There is significant evidence for low lying s-wave strength in many different experiments including the present data. The limits shown in Fig. 9 are shown in terms of the apparent peak energy. The original Kryger (1993) and Shimoura (1998) data were analyzed in terms of a Breit-Wigner

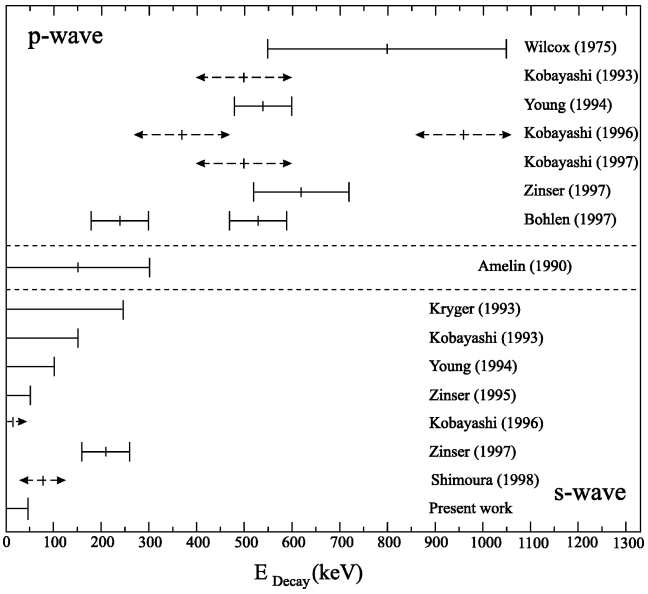

FIG. 9. Comparison of experimental results for p- and s-wave states. The s-wave states are presented in terms of apparent peak energies.

resonance and the apparent peak energies were derived from the ''resonance'' energies using the parametrization of Refs. [16] and [5], respectively. The Zinser (1995) data were analyzed in terms of a scattering length and the energy limit was calculated using the definition $E \simeq \hbar^2/2ma^2$ as in the original paper [20].

The recent data that were analyzed in terms of scattering length are in general agreement. Zinser (1995, $a_s < -20$ fm), Shimoura (1998, $a_s = -16^{+4}_{-7}$ fm), and the present data ($a_s < -20$ fm) all support the evidence for low-lying *s*-wave strength near the threshold in ^{10}Li.

Only the data of Ref. [3] seem inconsistent with the presence of very low-lying *s*-wave strength that necessarily must follow from a large numerical value of a_s. As discussed in [9] the theoretical spectrum of excitation energies in ^{10}Li from breakup of ^{11}Li on a light target rises much more steeply at low energy than does the measured spectrum. This explains why the fit [9] to the experimental data favors a numerically small value of $a_s = -1$ fm. The reason could be experimental as the shape of the onset of the structure is determined essentially by the single and lowest observed point near 0.05 MeV. Another effect that almost certainly must enter is that the observed peak at 210(5) keV in part or wholly reflects the 240 keV *p*-state that has been reported [4]. The likely presence of one more *p*-state peak in addition to the one at 540 keV will certainly make the analysis of the total energy spectrum less conclusive [3]. The present experiment on the other hand is by design especially sensitive to *s*-wave strength at the lowest energies due to its narrow acceptance in transverse momentum and should offer the best opportunity for this component.

Theoretically the situation is not clear. Many different approaches predict either *p*-wave ground states or low-lying *s*-wave strengths. A recent compilation of theoretical calculations of ^{10}Li can be found in Ref. [7]. One two-body (potential model) calculation predicts low-lying strength and quotes the results in terms of a scattering length [32]. The values of $a_s = -19$ fm ($J = 1^-$) and $a_s = -25$ fm ($J = 2^-$) are in agreement with the present data.

The limit of the scattering length of $a_s < -20$ fm also fits into the three body Fadeev calculations of ^{11}Li by Thompson and Zhukov [33]. In order to describe the properties of ^{11}Li they predict the scattering length as a function of the *p*-wave resonance and the mass of ^{11}Li [34]. The two shaded boxes in Fig. 10 correspond to the allowed regions limited by the measured ground state energy of ^{11}Li [15] and assuming a *p*-wave resonance in ^{10}Li at 538 ± 62 keV (\\\) [15], and 240 ± 60 keV (///) [4]. The dark shaded area shows the region of scattering lengths consistent with the present data which overlaps well with the limits set by the ^{11}Li mass and

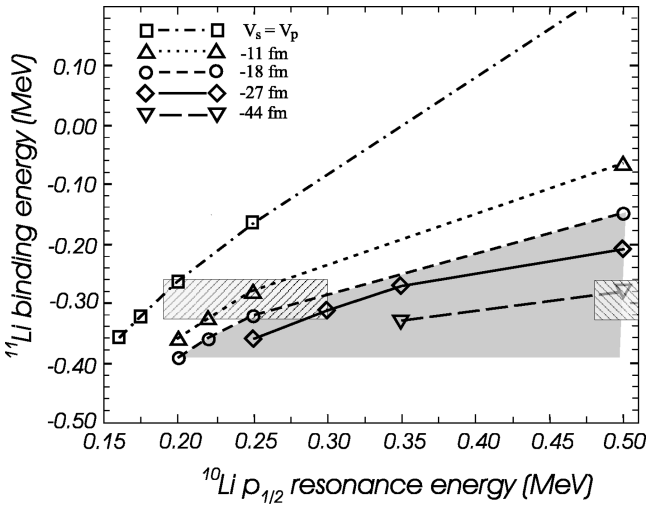

FIG. 10. Relation between the *s*-wave scattering length, the ^{11}Li binding energy and the ^{10}Li *p*-wave resonance energy. The figure was adapted from Ref. [33]. The hatched areas are experimental limits for the *p*-waves states from Refs. [15] (\\\), and [4] (///) within the limit of the ^{11}Li binding energy [34]. The dark shaded area corresponds to scattering lengths consistent with the present data.

the ^{10}Li *p*-wave resonance. Their apparent agreement with a measured momentum spectrum [35] cannot, however, be taken as direct support for this solution because of their simplified model of the reaction mechanism (final-state interactions [36] and the shadowing effect [37] were left out).

IV. CONCLUSIONS

The present data are in favor of low lying *s*-wave strength in ^{10}Li and thus demonstrates the continuation with decreasing *Z* of the parity inversion of *p*- and *s*-wave states which is also observed in ^{11}Be. Within a potential model a limit of the scattering length of < -20 fm was established.

Presently two questions remain. (i) A very low lying *p*-state cannot be ruled out, although it would contradict other evidence discussed above. In addition, a recent measurement at GSI of the angular distribution of the neutron with respect to the recoil direction seems to confirm the *s*-wave character of this low lying strength [38]. (ii) There is a possibility [16] that the presently measured decay energy could correspond to a decay from an excited state in ^{10}Li to the first excited and only bound state in ^{9}Li followed by γ-ray emission. Either an inverse kinematics transfer reaction like ^{9}Li(d,p) ^{10}Li or a coincidence measurement with γ rays should resolve this question. Both experiments were recently performed and the results should be available soon [39,40].

[1] T. Kobayashi, K. Yoshida, A. Ozawa, I. Tanihata, A. Korsheninnikov, E. Nikolsky, and T. Nakamura, Nucl. Phys. **A616**, 223c (1997).

[2] S. Shimoura *et al.*, Nucl. Phys. **A616**, 208c (1997).

[3] M. Zinser *et al.*, Nucl. Phys. **A619**, 151 (1997).

[4] H. G. Bohlen, W. von Oertzen, Th. Stolla, R. Kalpakchieva, B. Gebauer, M. Wilpert, Th. Wilpert, A. N. Ostrowski, S. M. Grimes, and T. N. Massey, Nucl. Phys. **A616**, 254c (1997).

[5] S. Shimoura *et al.*, Nucl. Phys. **A630**, 387c (1998).

[6] J. A. Caggiano, D. Bazin, W. Benenson, B. Davids, B. M.

Sherrill, M. Steiner, J. Yurkon, A. F. Zeller, and B. Blank (unpublished).
[7] P. Descouvemont, Nucl. Phys. **A626**, 647 (1997).
[8] S. Aoyama, K. Kato, and K. Ikeda, Phys. Lett. B **414**, 13 (1997).
[9] G. F. Bertsch, K. Hencken, and H. Esbensen, Phys. Rev. C **57**, 1366 (1998).
[10] P. G. Hansen, Nucl. Phys. **A630**, 285 (1998).
[11] B. A. Brown, in *Proceedings of the International School on Heavy Ion Physics, 4th Course: Exotic Nuclei*, edited by R. A. Broglia and P.G. Hansen (World Scientific, Singapore, 1998), p. 1.
[12] J. Wurzer and H. M. Hofmann, Z. Phys. A **354**, 135 (1996).
[13] K. H. Wilcox, R. B. Weisenmiller, G. J. Wozniak, N. A. Jelley, D. Ashery, and J. Cerny, Phys. Lett. **59B**, 142 (1975).
[14] H. G. Bohlen *et al.*, Z. Phys. A **344**, 381 (1993).
[15] B. M. Young *et al.*, Phys. Rev. C **49**, 279 (1994).
[16] R. A. Kryger *et al.*, Phys. Rev. C **47**, R2439 (1993).
[17] A. I. Amelin *et al.*, Yad. Fiz. **52**, 1231 (1990) [Sov. J. Nucl. Phys. **52**, 782 (1990)].
[18] T. Kobayashi, in *Proceedings of Radioactive Nuclear Beams III*, edited by D. J. Morrissey (Editions Frontieres, Gif-sur-Yvette, France, 1993) p. 169.
[19] T. Kobayashi, K. Tanaka, D. Smith, R. Ivie, P. Hui, and T. Fortune, RIKEN Accelerator Progress Report **29**, 79 (1996).
[20] M. Zinser *et al.*, Phys. Rev. Lett. **75**, 1719 (1995).
[21] J. H. Heltsley, L. Brandon, A. Galonsky, L. Heilbronn, B. A. Remington, S. Langer, A. Vandermolen, and J. Yurkon, Nucl. Instrum. Methods Phys. Res. A **263**, 441 (1988).
[22] F. Deák, A. Kiss, Z. Seres, G. Caskey, A. Galonsky, and B. Remington, Nucl. Instrum. Methods Phys. Res. A **258**, 67 (1987).
[23] A. M. Lane and R. G. Thomas, Rev. Mod. Phys. **30**, 257 (1958).
[24] A. S. Goldhaber, Phys. Lett. **70B**, 306 (1974).
[25] D. H. Boal, C. K. Gelbke, and B. K. Jennings, Rev. Mod. Phys. **62**, 553 (1990).
[26] W. Bauer, C. K. Gelbke, and S. Pratt, Annu. Rev. Nucl. Part. Sci. **42**, 77 (1992).
[27] S. Kowalski and H. A. Enge, RAYTRACE, Laboratory of Nucl. Sci. and Dept. of Physics, Massachusetts Inst. of Tech. (1987).
[28] R. A. Cecil, B. D. Anderson, and R. Madey, Nucl. Instrum. Methods **161**, 439 (1979).
[29] F. Ajzenberg-Selove, Nucl. Phys. **A490**, 1 (1988).
[30] R. D. Lawson, F. J. D. Serduke, and H. T. Fortune, Phys. Rev. C **14**, 1245 (1976).
[31] M. J. G. Borge *et al.*, Nucl. Phys. **A490**, 287 (1988).
[32] F. M. Nunes, I. J. Thompson, and R. C. Johnson, Nucl. Phys. **A596**, 171 (1996).
[33] I. J. Thompson and M. V. Zhukov, Phys. Rev. C **49**, 1904 (1994).
[34] B. M. Young *et al.*, Phys. Rev. Lett. **71**, 4124 (1993).
[35] N. A. Orr *et al.*, Phys. Rev. Lett. **69**, 2050 (1992).
[36] F. Barranco, E. Vigezzi, and R. A. Broglia, Phys. Lett. B **319**, 387 (1993).
[37] P. G. Hansen, Phys. Rev. Lett. **77**, 1016 (1996).
[38] D. Aleksandrov *et al.*, S135 Collaboration, GSI Scientific Report 1997, GSI 98-1, p. 16 (1998).
[39] J. Kolata *et al.*, NSCL Experiment 97003.
[40] M. Chartier *et al.*, in *Proceedings of the 2nd International Conference on Exotic Nuclei and Atomic Masses*, edited by B. M. Sherrill and D. J. Morrissey, AIP Conf. Proc. No. 455 (AIP, New York, 1998).